Exploring the Early Stages of the pH-Induced Conformational Change of Influenza Hemagglutinin

ARTICLE *in* PROTEINS STRUCTURE FUNCTION AND BIOINFORMATICS · OCTOBER 2014

Impact Factor: 2.63 · DOI: 10.1002/prot.24606

4 AUTHORS:

Yu Zhou
National Institute of Biological Sciences, China
5 PUBLICATIONS **6** CITATIONS
SEE PROFILE

Chao Wu
Washington University in St. Louis
1 PUBLICATION **4** CITATIONS
SEE PROFILE

Lifeng Zhao
National Institute of Biological Sciences, China
12 PUBLICATIONS **87** CITATIONS
SEE PROFILE

Niu Huang
National Institute of Biological Sciences, China
52 PUBLICATIONS **2,029** CITATIONS
SEE PROFILE

PROTEINS
STRUCTURE ■ FUNCTION ■ BIOINFORMATICS

Exploring the early stages of the pH-induced conformational change of influenza hemagglutinin

Yu Zhou,[1,2] Chao Wu,[2,3] Lifeng Zhao,[2] and Niu Huang[1,2]*

[1] College of Life Sciences, Beijing Normal University, Beijing 100875, China

[2] National Institute of Biological Sciences, Beijing, Zhongguancun Life Science Park, Beijing 102206, China

[3] Department of Biochemistry and Molecular Biophysics, Washington University School of Medicine, St. Louis, Missouri 63110

ABSTRACT

Hemagglutinin (HA) mediates the membrane fusion process of influenza virus through its pH-induced conformational change. However, it remains challenging to study its structure reorganization pathways in atomic details. Here, we first applied continuous constant pH molecular dynamics approach to predict the pK_a values of titratable residues in H2 subtype HA. The calculated net-charges in HA1 globular heads increase from 0e (pH 7.5) to +14e (pH 4.5), indicating that the charge repulsion drives the detrimerization of HA globular domains. In HA2 stem regions, critical pH sensors, such as $Glu103_2$, $His18_1$, and $Glu89_1$, are identified to facilitate the essential structural reorganizations in the fusing pathways, including fusion peptide release and interhelical loop transition. To probe the contribution of identified pH sensors and unveil the early steps of pH-induced conformational change, we carried out conventional molecular dynamics simulations in explicit water with determined protonation state for each titratable residue in different environmental pH conditions. Particularly, energy barriers involving previously uncharacterized hydrogen bonds and hydrophobic interactions are identified in the fusion peptide release pathway. Nevertheless, comprehensive comparisons across HA family members indicate that different HA subtypes might employ diverse pH sensor groups along with different fusion pathways. Finally, we explored the fusion inhibition mechanism of antibody CR6261 and small molecular inhibitor TBHQ, and discovered a novel druggable pocket in H2 and H5 subtypes. Our results provide the underlying mechanism for the pH-driven conformational changes and also novel insight for anti-flu drug development.

Proteins 2014; 00:000–000.

Key words: influenza hemagglutinin; pH-induced conformational change; continuous constant pH molecular dynamics; molecular dynamics simulation; fusion inhibitor.

INTRODUCTION

Influenza virus has presented serious threats to public health worldwide and growing concerns have been raised about the evolution of the highly pathogenic avian influenza (HPAI) H5N1,[1–4] H7N7[5,6] viruses and recent H7N9[7,8] virus spreading in China. Hemagglutinin (HA) plays an essential role in the life cycle of influenza virus. It is responsible for the binding to sialic acid receptors during the initial stages of infection, and membrane fusion between viral envelope and endosomal membrane after virus uptake into endosomes.[9] HA is a homotrimer glycoprotein with each monomer consisting of two disulfide bond-linked chains (HA1 and HA2 subunits). The native structure of HA comprises a large membrane-distal, globular head domain binding to glycan receptors on host cells and an elongated membrane-proximal domain (also called stem region) dominated by intertwined and interconnecting α-helices [Fig. 1(A)].[10] The HA-mediated membrane fusion works through its extensive conformational change, which are triggered at acidic pH in the endosome. Comparison of structures at neutral pH (pH 7.4) and fusion pH (pH 5.0, HA2 ectodomain) indicates that the

Additional Supporting Information may be found in the online version of this article.

Grant sponsor: Chinese Ministry of Science and Technology "973" (N.H.); Grant number: 2011CB812402.; Grant sponsor: Supercomputing Center of Chinese Academy of Sciences (SCCAS).

*Correspondence to: Niu Huang, National Institute of Biological Sciences, Beijing, No. 7 Science Park Road, Zhongguancun Life Science Park, Beijing 102206, China. E-mail: huangniu@nibs.ac.cn

Received 23 January 2014; Revised 15 April 2014; Accepted 12 May 2014
Published online 23 May 2014 in Wiley Online Library (wileyonlinelibrary.com).
DOI: 10.1002/prot.24606

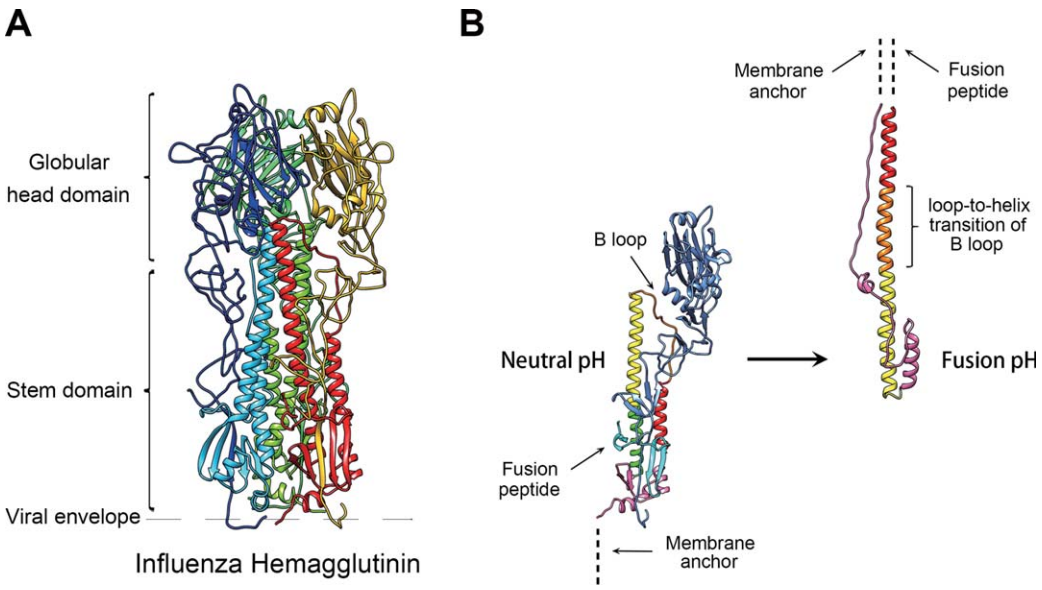

Figure 1

(**A**) Structure of the HA trimer at neutral pH (PDB ID: 2HMG). (**B**) pH-induced conformational change of HA. Only one monomer of the trimer is shown for clarity. The neutral pH structure (left) is from PDB 2HMG and the fusion pH structure is from PDB 1HTM. In PDB 1HTM, only HA2 subunit was determined. Molecular images were generated using UCSF Chimera. [Color figure can be viewed in the online issue, which is available at wileyonlinelibrary.com.]

HA1 globular heads detrimerize at low pH.[10,11] The short α-helix of HA2 is repositioned onto the long α-helix by refolding of the interhelical loop (B loop), forming a new α-helix extended 100 Å long. The fusion peptide in the N-terminus of HA2 is relocated from the buried trimer interface toward the membrane-distal direction to facilitate its later insertion into the endosomal membrane [Fig. 1(B)].

Several models have been proposed for the mechanism of pH-induced HA conformational change. The most widely accepted model, spring-loaded model,[12,13] suggests the native structure of HA is trapped in a metastable state and the fusogenic conformation is released by destabilizing the native structure, where the pH is the sole trigger. The enhanced protonation of HA at low pH would lead to electrostatic repulsion between globular heads and lowering the stability of the trimeric association;[14,15] however, it is not clear which key residues are protonated and initiate the conformational change. Many mutations affecting the fusion pH have been characterized in HA,[16–29] with most of them locating surrounding the fusion peptide and HA1-HA2 interface. Although these mutagenesis studies have provided informative clues, it is still difficult to identify the critical pH sensors. The pK_a values of titratable residues are largely dependent on their local environments, and their protonation states are difficult to be directly measured by currently available experimental techniques. Besides, the abundant titratable residues in various HA subtypes throughout evolution further complicate detailed characterization by traditional sequence-based analysis and mutagenesis studies.[30]

Structural study of the fusion intermediates is also challenging, given their transient nature. Several indirect methods have been applied to investigate the potential pathways of the HA structure reorganization. For example, a panel of antipeptide antibodies was used to probe important regions of H3 subtype HA in response to low pH.[31] Such kinetic studies indicated that the stem interface loop becomes exposed from the trimer interface quickly followed by the fusion peptide, and then the HA1 globular domains become more accessible to their corresponding antisera exposing the interhelical loop. In addition, studies of H3 subtype HA using double mutants further showed that there are at least three events in the refolding pathway: fusion peptide release, destabilization of adjacent short α-helix, and dissociation of HA1 from HA2.[32] Electron cryomicroscopy structure of H2 subtype HA at fusion pH indicates the formation of a central cavity through the entire ectodomain by rearrangements of the tertiary structure in the distal and the stem regions.[33] Examination of the effects of low pH treatment on H2 and H3 HA subtypes also suggests different conformational states after exposure at low pH.[34] Encouragingly, crystal structure of an early fusion intermediate of H2 mutant (HA2R106H) was recently determined.[30] It provided the first atomic-resolution snapshot of putative fusion intermediate, in which the interhelical loop moves away from the central helical bundle and adopts a relatively loose conformation. All

these experimental studies mapped out the fusion pathway to certain extents; however, full characterization of the pH sensing mechanism and structure reorganization pathway has awaited more atomic level descriptions of the conformational change.

In this work, we computationally investigated the atomic details of this pH-induced HA conformational change. First, we applied continuous constant pH molecular dynamics (CPHMD) simulations[35–37] to calculate the pK_a values of titratable residues in neutral-pH H2 HA structure and low-pH H2_HA2R106H mutant structure. Based on the computed pK_a values, we determined the protonation state of titratable residues at different environmental pH values, and we carried out conventional MD simulations to study the conformational change at different pH conditions, individually. We also attempted to mimic the protonation equilibrium by iteratively combining conventional MD simulations with pK_a calculations in a discrete way. Our results indicate the underlying mechanism of the pH-induced HA conformational change and support the spring-loaded model at atomic details. We identified several critical titratable residues as potential pH sensors to initiate this process, including $Glu103_2$, $His18_1$, and $Glu89_1$. And the dynamic behaviors of initial stages of conformational change were captured in the conventional MD simulation. The protonation of these pH sensors disrupts the hydrogen bond network and introduces local perturbation to initiate the conformational change. In addition, we performed comprehensive comparisons across HA family members, which strongly suggest that diverse pH sensor groups and fusion pathways might exist in different HA subtypes. Since interfering with pH-induced conformational change of influenza HA has been proved to be an efficient way for the inhibition of virus infection, our studies also provide new insights into the design of selective HA inhibitors.

MATERIALS AND METHODS

HA subtypes

With the most recent H17 and H18 being discovered in bats,[38,39] there are total of 18 HA subtypes (H1-H18) of influenza A viruses and they could be phylogenetically divided into two groups (see the Supporting Information, Fig. S1). To make a comprehensive comparison, we carried out CPHMD simulations for all representative subtypes with available structures, plus the recently reported low pH intermediate of H2_HA2R106H mutant. For each HA subtype, we selected a high-quality X-ray crystal structure from the Protein Data Bank (PDB)[40] as initial coordinates (PDB IDs are provided in the Supporting Information, Table SI). Since the H16 HA structure is in the uncleaved (HA0) form,[41] and the N-terminus of fusion peptide in both H17 and H18 HAs are not well-determined,[39,42,43] they were excluded in our study. For the long-time conventional MD simulation, we just performed on three different HA subtypes (H2/H3/H5) due to limited resource. H2 and H3 represent two distinct HA lineages and both of their corresponding viruses are responsible for human influenza pandemics.[44] H5 is the closest HA subtype to H2 and its corresponding virus (H5N1) has also presented a serious threat to human health.[1,45]

Constant pH molecular dynamics simulations

We carried out CPHMD simulations using CHARMM molecular dynamics program (version 35b2).[46] The replica-exchange (REX) protocol was enabled through the MMTSB tool set[47] to obtain enhanced conformational and protonation state sampling. We used the CHARMM 22 all-atom protein force field,[48] including the dihedral cross-term corrections (CMAP)[49] and optimized GB input radii set.[50] The optimal pH range for membrane fusion by HA is around 5–5.5, and pH 4.5 is widely used in *in vitro* experimental studies.[31] In our study, we chose pH 4.5 as the lower bound, and used pH 7.5 to represent the neutral pH. For each system, simulations were initiated at four different pH conditions at one unit interval (pH = 7.5, 6.5, 5.5 and 4.5). A REX simulation at each pH used 40 replicas occupying a temperature scale from 298 to 400 K. A conformational exchange was attempted every 1 ps between replicas adjacent in temperature with an acceptance ratio of 40–60%. Each replica was subjected to a constant pH, volume, and particle MD run for 400 ps. In our system, 400 ps simulation is enough to generate converged results, and the results are comparable with that from 1000 ps simulation (data not shown). The SHAKE algorithm[51] was applied to hydrogen bonds allows a 2 fs time step, and a 22 Å distance truncation was applied to the nonbonded and GB energy/force evaluation. The salt concentration was fixed at 0.15*M* in all simulations to represent typical salt concentration in experimental studies. The side chains of all Asp, Glu, His, Lys, and Arg residues were allowed to titrate during simulation. Cys residues in HA are not considered since they all form disulfide bonds. The α-amino of residue Gly_1 in HA2 was also allowed to titrate since it is the N-terminus of the fusion peptide and is buried in the conserved stem region. Other N-terminal amino and C-terminal carboxyl groups were blocked by acetyl (ACE) and N-methylamide (NME) groups, respectively. We derived the model PMF parameters for the titratable N-terminus of Gly residue (Supporting Information, Table SII). The force field parameter for TBHQ is generated using CGenFF program.[52,53] In the H3-TBHQ complex system, a 5 kcal mol^{-1} $Å^{-2}$ harmonic position restraint was applied on

the heavy atoms of TBHQ molecule to stabilize it in the binding site during the high-temperature simulations.

The pK_a values of all titratable residues could be computed by analyzing the titration data from REX-CPHMD simulations. The fractional population of unprotonated states S^u is given by $S^u \approx N^u/(N^u+N^P)$. After obtaining S^u of a titratable residue at different pH conditions, the pK_a value is obtained by fitting the generalized form of the Henderson–Hasselbalch equation : $S^u = 1/(1+10^{n(pKa-pH)})$, where n is the Hill coefficient. The homotrimer configuration of HA allows us to take advantage of multicopy sampling, amounting to the equivalent of threefold 400 ps sampling for each HA monomer, while accounting for realistic neighboring subunit effect within the dynamics. The final pK_a value of each titratable residue is an averaged value in two monomers with smaller deviation to minimize the potential error brought by an outlier. This data processing method generally resulted pK_a values with a deviation less than 0.3 pH unit.

Conventional molecular dynamics simulations

All the systems for conventional MD simulations were setup as follows. Protonation state for each titritable residue was assigned based on the pK_a predictions from CPHMD simulations. Residues with calculated pK_a values greater than (or equal to) the environment pH were treated as protonated. Their tautomeric states were also referred to the CPHMD results. For each structure, we carried out four independent simulations at different pH conditions (pH = 7.5, 6.5, 5.5 and 4.5). All systems were setup using the Schrödinger software. CHARMM 22 all-atom force filed was assigned to protein with CMAP correction. A 15 Å buffered orthorhombic boundary system was built with TIP3P water and then neutralized by counter ions.

All MD simulations were performed using the Desmond 2.2 software package.[54] Each system was minimized using 5000 steps of steepest descent algorithm with gradually reduced restraint. Following minimization, the system was gradually heated to 300 K in the canonical NPT ensemble using a Berendsen thermostat,[55] with a 50 kcal mol^{-1} $Å^{-2}$ harmonic position restraint applied to all heavy atoms of the protein. The restraints were gradually removed and the production run was performed in MTK-NPT (1 bar, 300 K) ensemble for 100 ns. The M-SHAKE algorithm was applied to constrain all bonds involving hydrogen atoms with a time step of 2 fs. The short-range electrostatic and Lennard–Jones interactions were cut off at 9 Å. Long-range electrostatic interactions were computed by the particle mesh Ewald method[56] using a 64 × 64 × 64 grid with σ equal to 2.18 Å. Structural analysis was performed using the UCSF Chimera[57] and VMD[58] programs.

Table I
Calculated pK_a Values for H2 HA Titratable Residues at T = 298 K

pKa values[a]	Residues in H2 HA[b]
>7.5	N-ter $Gly1_2$[c], all Arg, all Lys, and $Hip38_1$[d]
7.5	$Hip142_2$
6.8	$Hie25_2$
6.3	$Hie47_1$, $Glu216_1$
6.2	$Glu89_1$, $Hie116A_1$
6.1	$Glu103_2$
5.8	$Asp11_1$
5.7	$Hie130_1$
5.6	$Hie26_2$
5.3	$Asp187_1$
5.0	$Glu75_1$, $Asp95_1$, $Hie183_1$, $Glu163_2$
4.8	$Asp27_1$, $Glu271_1$
4.7	$Hid18_1$, $Glu174_1$, $Glu190_1$, $Glu105_2$
4.6	$Asp104_1$, $Glu304_1$
4.5	$Glu24_1$, $Asp109_2$, $Hie111_2$, $Glu172_2$
< 4.5	All the other Asp, all the other Glu, $Hie110_1$, $Hie184_1$, $Hie295_1$, and $Hie298_1$

[a]The Henderson–Hasselbach (HH) equation is fitted in the range of 4.5–7.5.
[b]Each residue is numbered according to the H3 HA number. The subscript numbers denote the HA subunits.
[c]N terminus amide group of $Gly1_2$ in fusion peptide.
[d]Three different protonation states exist in histidine residues: Hip, double protonated; Hid, N_δ protonated; Hie, N_ϵ protonated.

RESULTS AND DISCUSSION

Charge repulsion driving the detrimerization of globular heads

The pK_a values of all titratable residues in HA were computed by analyzing the titration data from CPHMD simulations. The results of H2 HA are summarized in Table I. The calculated pK_a values of all arginine, lysine residues, and the amino-terminus of fusion peptide in H2 HA are greater than 7.5, and thus they were protonated in the pH range of our interest. Histidine residues (pK_a value of isolated histidine is 6.5) are generally assumed to be of particular importance in pH-regulated biological phenomena.[59,60] There are 14 histidine residues in each H2 HA monomer. Our results suggest their calculated pK_a values are highly dependent on the local environment and span a large pH range. The pK_a values of isolated aspartic acid and glutamic acid are 4.0 and 4.4, individually. Interestingly, the calculated pK_a values of several aspartic acid and glutamic acid residues in H2 HA are significantly up-shifted (e.g., the calculated pK_a value of $Glu103_2$ is 6.1); therefore, it is protonated at the fusion pH.

HA undergoes conformational change in response to the decreasing pH. As the environmental pH decreases, titratable residues with pK_a value greater than the environmental pH will be protonated, and bring positive charges into the protein system. Thus, we could theoretically predict the order of protonation events in HA by performing CPHMD simulations at different environmental pH conditions. A series of titratable residues throughout H2 HA got protonated sequentially as the

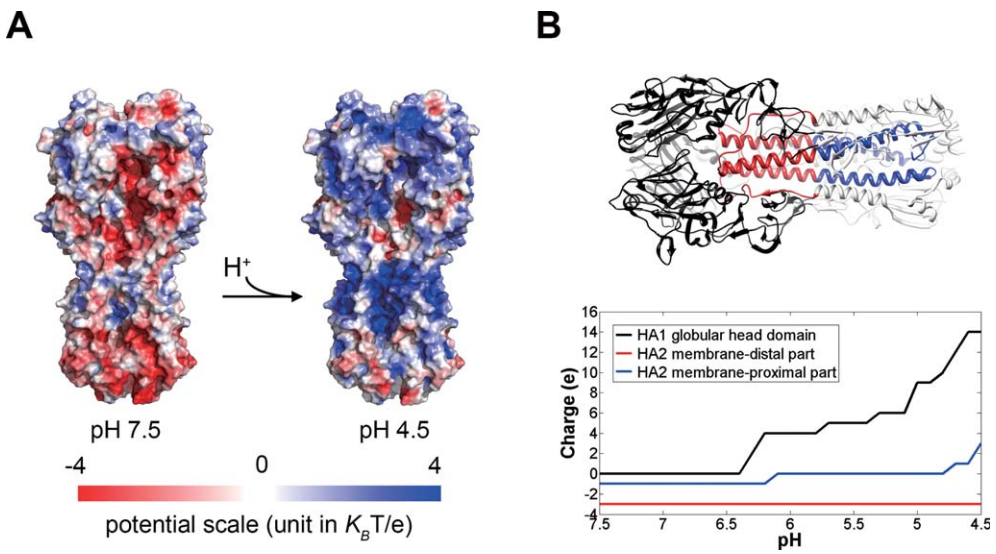

Figure 2

Alternation of charge distribution induced by low pH. (**A**) Surface electrostatic potential of H2 HA at pH 7.5 and at pH 4.5. It is generated based on the calculated pK_a value using the PyMOL APBS Plugin.[61] Red represents negative electrostatic potential, blue represent positive electrostatic potential, and white is neutral. (**B**) Net charge of three specific regions in H2 HA as a function of pH. HA1 globular head domain (residues 42_1-314_1) is colored in black, containing the receptor-binding domain and a vestigial esterase domain; HA2 membrane-distal part (residues 56_2-99_2) colored in red denotes the interhelix loop and the membrane-distal part of long α-helix; HA2 membrane-proximal part (residues 100_2-135_2) colored in blue denotes the membrane-proximal part of long α-helix surrounding the fusion peptide.

pH decreases from 7.5 to 4.5 (see the Supporting Information, Fig. S2). Nevertheless, most protonated residues are located in the HA1 globular head domain or the HA2 fusion peptide cavity region, which is clearly demonstrated by using the surface electrostatic potential and the protein's net charge calculated under different environmental pH conditions (Fig. 2).

To decompose the contributions of different domains, we analyzed the charge distributions of three specific regions [Fig. 2(B)]. Accordingly, the HA1 globular head domains are electrostatically neutral at pH 7.5 (with net charge of 0e). When the pH reaches 4.5, the HA1 globular head domains become highly positively charged (with net charge of +14e). Thus, they will experience significant repulsion from each other, which results in the dissociation of HA1 globular domains to release the unfavorable electrostatic repulsion energy. In the membrane-proximal regions surrounding the fusion peptide, we observed a similar but relatively small change of net charge. The net charge is −1e at pH = 7.5, and +3e at pH = 4.5. The change of net charge on this region may also help destabilize the monomer interfaces, enlarge the cleft to facilitate the fusion peptide release, and the inflow of water solvents to protonate less exposed titratable residues previously. The connecting interhelical loop (B loop) between two antiparallel helices of HA2 subunits has a high propensity for a helical conformation and transforms into part of a long α-helix in the postfusion HA.[11,12] This loop-to-helix transition could form spontaneously at neutral pH as well in the absence of HA1 subunit.[13,62] Our results indicate that the net charge in the B loop region does not change, thus the B loop is likely trapped in a metastable conformation in the prefusion state as proposed by spring-loaded model, and acidification may be simply required for other steps of HA conformational change to release the clamp.

Our calculated net charges are consistent with previous experimental observation[14,33] and reveal the physical basis for the low-pH-induced conformational change of HA. The enhanced protonation at fusion pH increases the net charge of HA and generates local charge repulsion to initiate the structure reorganization. However, question arises here that: is the fusion process triggered by the general effects of an increased net charge or by the protonation of one or more critical titratable residues? To study the protonation effects in microscopic details, we mapped the titratable residues onto the H2 HA structure. For protonated residues located in the HA1 globular head domains, no particular interactions with adjacent residues were observed; and we also found many of these residues locating in the monomer interfaces of the HA1 globular head domains [Supporting Information, Fig. S2(D)]. Therefore, the dissociation of the HA1 globular head domains may simply be caused by the increased overall surface charges. Nevertheless, we did identify several titratable residues involving in important interaction networks surrounding the HA2 fusion peptide cavity. They may function as pH sensors and will

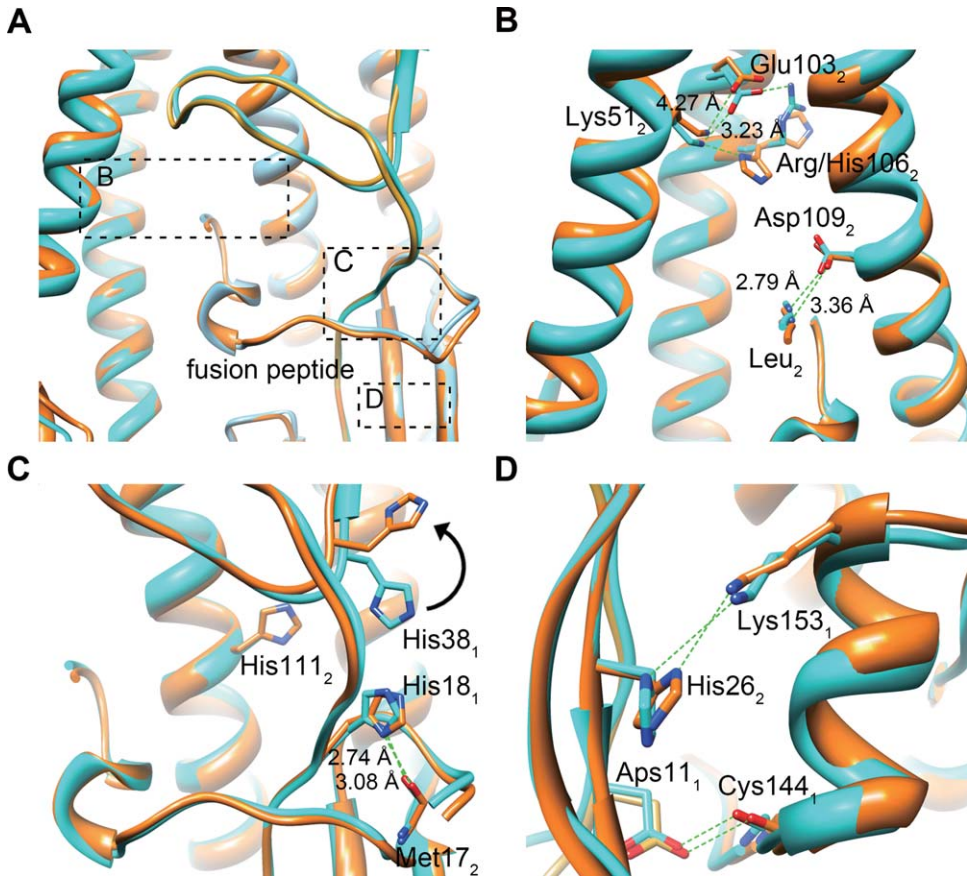

Figure 3

pH sensor groups facilitate the release of fusion peptide. Structure of neutral H2 HA (PDB ID: 3KU5) is colored in cyan, and structure of low pH intermediate H2_HA2R106 mutant (PDB ID: 3QQO) is colored in orange.

be discussed in greater details in the following subsection. This observation is consistent with the evolution of HA genes. The HA1 globular head domain is a hypervariable region during evolution, thus unlikely to preserve conserved pH sensor groups. While the stem region, which is quite conserved among different HA subtypes, may share common pH sensor groups to control the fusion related conformational change. Besides, the change of net charge is much smaller in the stem region, indicating that a few critical titratable residues may play essential roles in response to low pH.

We note that all calculated pK_a values in Table I are obtained based on the structure of neutral-pH H2 HA. However, it is well-known that conformational change of the structure would affect the local environment of these titratable residues; therefore, perturbing their protonation states, which could in turn accelerate the further conformational change. To further investigate the potential late stage protonation events, we also carried out CPHMD-pK_a calculations on the crystal structure of low pH intermediate and MD simulation snapshots.

Potential pH sensor groups facilitate the fusion process

A recently solved crystal structure of an early fusion intermediate of H2 mutant (HA2R106H) provides a unique opportunity for us to identify the potential pH sensor groups at this trapped conformational state. Their calculated pK_a values are provided in Supporting Information, Table SIII. Not only the observed structural transitions in this low pH intermediate would confirm our calculations based on the neutral-pH wild type H2 HA, but also the calculated pK_a shifts between these two configurations could reveal the conformational effect on the protonation states, which may help us identify new critical pH sensors.

Fusion peptides are originally deeply buried into the cleft of helices from two neighboring monomers [Fig. 3(A)], and have to be released from the cavity at fusion pH. Several potential pH sensor groups have been identified to facilitate its release. Above the N-terminus of the fusion peptide, Glu103$_2$ forms salt bridge interactions with nearby Lys51$_2$ and Arg106$_2$, which hold the short

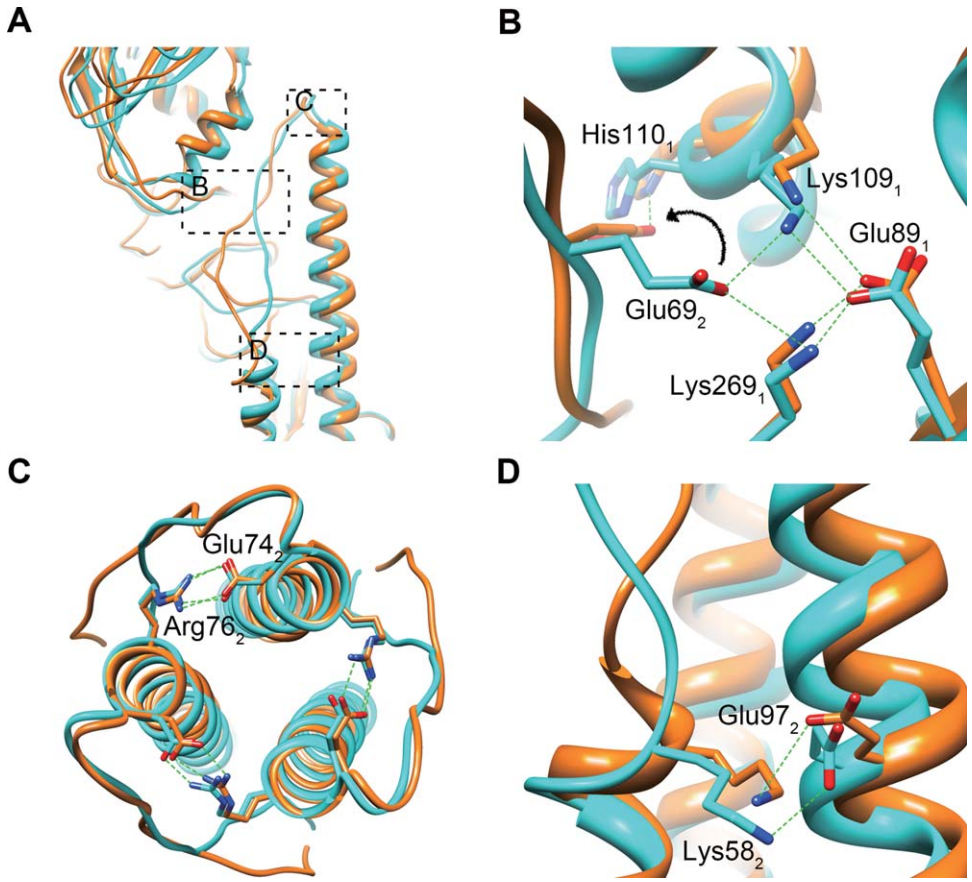

Figure 4

pH sensor groups facilitate the transition of interhelical B loop. Structure of neutral H2 HA (PDB ID: 3KU5) is colored in cyan, and structure of low pH intermediate H2_HA2R106 mutant (PDB ID: 3QQO) is colored in orange.

and long α-helix together in the neutral pH structure [Fig. 3(B)]. According to our calculation, the pK_a value of Glu103$_2$ is 6.2. Thus, Glu103$_2$ is protonated at low pH conditions and disrupts its original favorable interactions. The short α-helix would become easier to dissociate from the long α-helix, exposing the fusion peptide cavity. Besides, the calculated pK_a of Asp109$_2$ is up-shifted from 4.5 in neutral-pH crystal structure to 5.6 in low-pH intermediate crystal structure (Supporting Information, Table SIII). The protonation of Asp109$_2$ will further remove a hydrogen bond to the backbone amide of Leu2$_2$ of the fusion peptide [Fig. 3(B)] and thus facilitate the release of fusion peptide. Substitution of Asp109$_2$ with Ala/Gly/Glu in H3 HA has also indicated that directly destroying this hydrogen bond with fusion peptide would destabilize the HA and result in an elevated fusion pH by 0.2–0.4 unit.[27] Adjacent to the middle part of the fusion peptide, His18$_1$ (with an up-shifted pK_a from 4.7 to 6.0) is also protonated in the low pH condition, resulting in the loss of a hydrogen bond to the backbone carbonyl of Met17$_2$ in the fusion peptide and thus assisting its release [Fig. 3(C)]. In addition, this positively charged His18$_1$ produces strong repulsion with the neighboring positively charged His38$_1$ (with a calculated pK_a of 7.8), leading to the flipping of His38$_1$. This has also been observed in low-pH intermediate and is consistent with previous mutagenesis study. H18$_1$Q substitution in H5, maintaining the hydrogen bond with fusion peptide and losing the ability to get protonated at low pH, stabilized the HA and decreased the fusion pH by 0.4 unit.[28] At the membrane proximal region of the fusion peptide, both His26$_2$ (with a calculated pK_a of 5.6) and Asp11$_1$ (with a calculated pK_a of 5.8) would also be protonated at low pH, disrupting corresponding hydrogen bonds with Lys153$_1$ and Cys144$_1$, respectively [Fig. 3(D)]. This would further facilitate the relocation of the fusion peptide and refolding of HA2 C-terminal domain.

In the neutral-pH structure, the interhelical B loop is clamped by HA1 subunit and stabilized by interactions with adjacent residues [Fig. 4(A)]. Among many interactions, there is a conserved tetrad salt bridge network

including residues $Glu89_1$, $Lys109_1$, $Glu69_2$, and $Lys269_1$ [Fig. 4(B)]. Mutagenesis study in H3 HA has demonstrated the interruption of this charge quartet (substitution by Glu or Gly at position 109_1 or 269_1) weakens the stability of the prefusion trimer.[25] Protonation of $Glu69_2$ has previously been proposed to be the driving force for the B loop transition.[30] However, our pK_a calculation results suggest that $Glu69_2$ is not likely protonated at the initial stage. The calculated pK_a of $Glu69_2$ is less than 4.5 in both neutral and low pH H2 HA structures. Instead, we found $Glu89_1$ has a largely up-shifted pK_a of 6.2 in neutral pH structure. Thus, $Glu89_1$ will be protonated at low pH to interrupt the tetrad salt bridge network [Fig. 4(B)]. Further rotation of the B loop might require the destabilization of another two salt bridges located on its two ends. At the top of the B loop, three intersubunit salt bridges formed between $Glu74_2$ and $Arg76_2$ are shielded by the HA1 globular head domains [Fig. 4(C)]. And $Glu97_2$, located in the bottom of the B loop and interacts with $Lys58_2$ [Fig. 4(D)].It is not obvious that whether these two glutamic acid residues act as critical pH sensors to release the B loop.

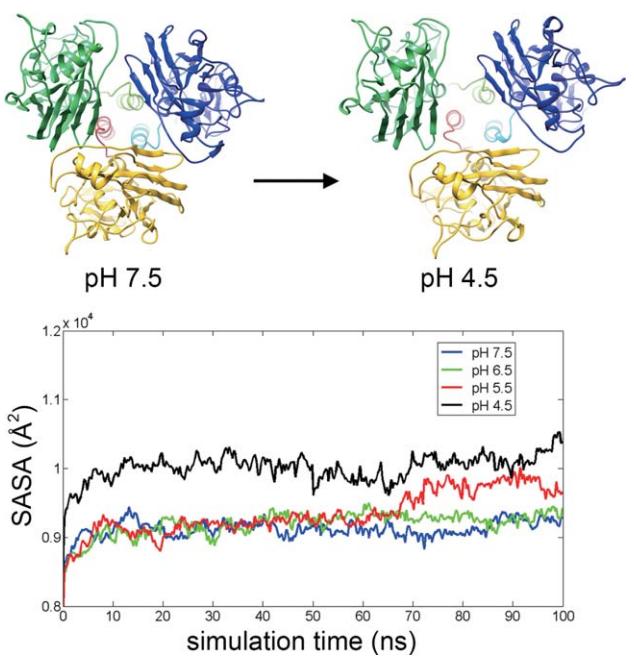

Figure 5

Detrimerization of globular head domains of H2 HA in low pH simulations. [Color figure can be viewed in the online issue, which is available at wileyonlinelibrary.com.]

Dynamics of HA conformational change

To probe the pH effects on HA dynamic behaviors at the atomic level, we carried out four 100 ns MD simulations for H2 HA at different pH conditions. At each pH condition, we assigned the protonation states for all titratable residues based on our pK_a predictions. Root mean square deviation (RMSD) calculations of alpha-carbon atoms suggest equilibriums are reached for all systems after 100 ns, and there are good agreements between crystal and simulation-derived B factors at the neutral pH (see the Supporting Information, Fig. SIII).

As the pH decreases, the most significant conformational change is the detrimerization of globular head domains (Fig. 5). This is consistent with experimental observations and our calculated net charges at different pH conditions. The solvent accessible surface area (SASA) plots show that three globular head domains pack tightly with each other at pH 7.5 and 6.5. When the pH decreases to 5.5, globular head domains start to dissociate from each other after 70 ns and are exposed to the solvent with an increased ΔSASA of 650 $Å^2$ for each monomer. In the simulation at pH 4.5, globular head domains dissociate from each other very quickly and the ΔSASA for each monomer is about 1000 $Å^2$. Clearly, the enhanced protonation at fusion pH introduces the electrostatic repulsion, and leads to the dissociation of globular head domains. Interestingly, during the detrimerization process, the globular head domains in each monomer experience small structural fluctuation, with an RMSD of 0.9 Å for all Cα atoms in this region.

The fusion peptides in the stem region begin to move out of the cavity and are exposed to the solvent at low pH [Fig. 6(A)]. In the neutral-pH structure, fusion peptide is deeply buried and participates in a hydrogen bond network with surrounding residues, holding it tightly in the cavity. Protonation of relevant residues in this area would perturb these hydrogen bonds; subsequently facilitate the fusion peptide releasing. For example, $Asp109_2$ forms hydrogen bond with the backbone amide of $Leu2_2$ of the fusion peptide in the neutral-pH structure, which is disrupted by the protonation of $Asp109_2$ at low pH (pH 4.5) [Fig. 6(B)]. Losing this hydrogen bonding interaction, the fusion peptide will move out of the cavity much more easily. Total of 12 hydrogen bonds are presented with the fusion peptide in the H2 HA crystal structure [Fig. 6(C)], all of which are required to be broken to relocate the fusion peptide at fusion pH. However, in the 100 ns simulation at pH 4.5, we only observed six hydrogen bonds are broken [see the occupancy calculations at different pH conditions in Fig. 6(C)]. The others are still remaining stable during the 100 ns simulation, four of which interacting with $Asp112_2$. Further releasing of fusion peptide requires the breakage of these remaining hydrogen bonds. The protonation of $Asp112_2$ would greatly accelerate this process.

Our simulations also indicate the presence of two major hydrophobic barriers along fusion peptide release pathway at the early stages. In the crystal structure, $Ile6_2$ and $Phe9_2$ of the fusion peptide pack well with the side chain of nearby $Tyr17_1$ and $Tyr119_2$, respectively [Fig.

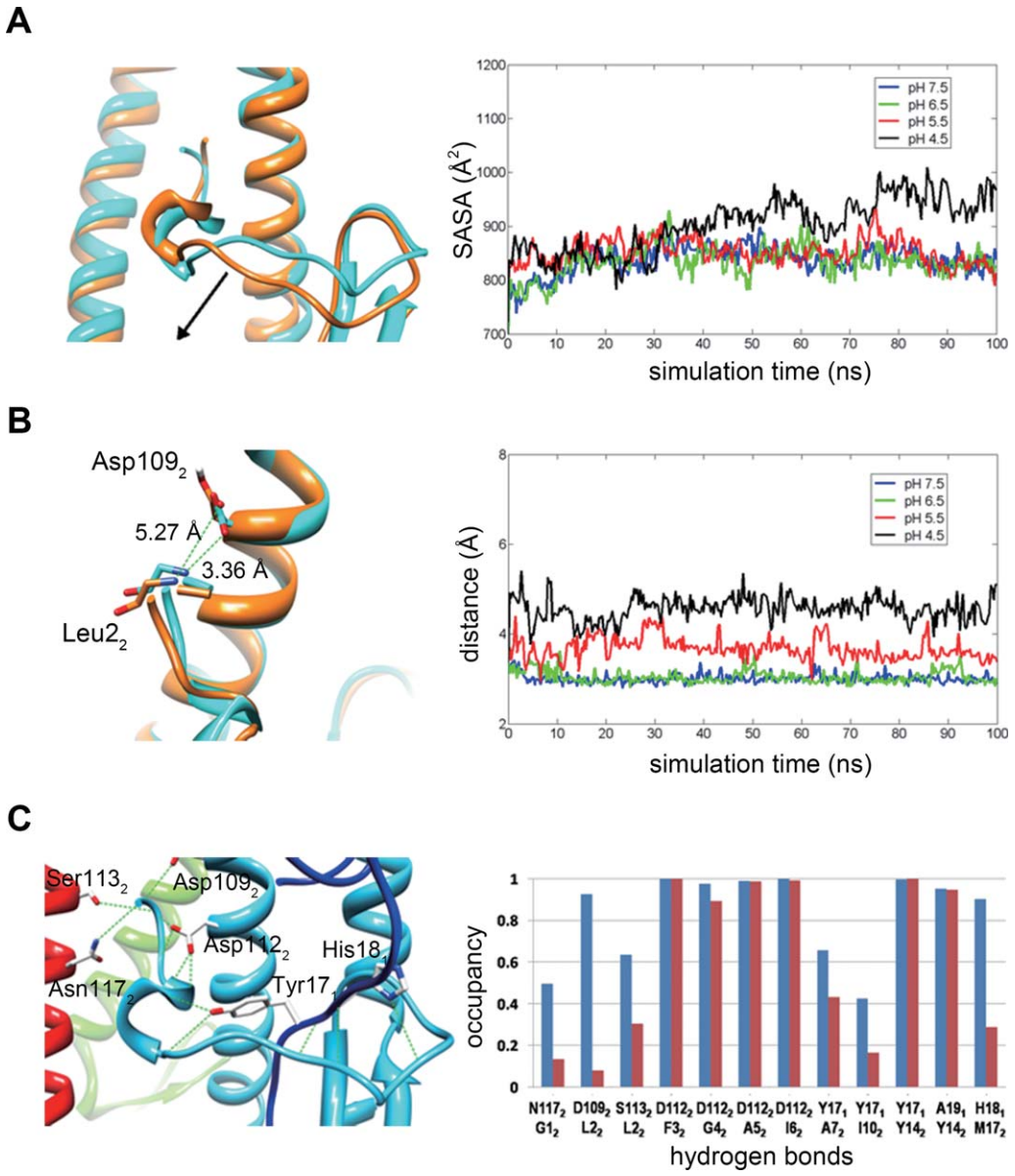

Figure 6

Analysis of the hydrogen bond interaction network with the fusion peptide in H2 HA simulation. (**A**) Solvent accessible surface area (SASA) of fusion peptide (residues 1_2-20_2) during 100 ns simulations at different pH conditions. Conformation at pH 7.5 is shown in cyan and that at pH 4.5 is shown in orange. (**B**) Analysis of the hydrogen bond distance between $Asp109_2$ and $Leu2_2$ at different pH conditions. Conformation at pH 7.5 is shown in cyan and that at pH 4.5 is shown in orange. (**C**) Occupancy calculation of the hydrogen bonds interaction network during the simulations at different pH conditions. Blue: at pH 7.5; red: at pH 4.5. [Color figure can be viewed in the online issue, which is available at wileyonlinelibrary.com.]

7(A)]. At pH 4.5, with the perturbation brought by the protonation of $Asp109_2$ and $His18_1$ in this region, $Phe9_2$ first flips out of the cavity after 54 ns simulation, and instead the adjacent $Ile10_2$ participates in the packing with $Tyr119_2$ side chain [Fig. 7(B)]. After 75 ns simulation, $Ile6_2$ then rotates away from $Tyr17_1$, further loosening the fusion peptide [Fig. 7(C)]. Finally, the $Ile10_2$ residue is also released from the packing with $Tyr119_2$ after 91 ns simulation [Fig. 7(D)]. Therefore, the fusion peptide moves out of the cavity step by step, getting across the energy barriers consisting of hydrophobic packing and hydrogen bonding interactions.

Accompanying the fusion peptide release, we also observed the separation of short and long α-helices in low pH simulations [Fig. 8(A)]. The salt bridge between $Glu103_2$ and $Lys51_2$ is stable at neutral pH, with a distance of 2.79 Å. The protonation of $Glu103_2$ (with calculated pK_a of 6.1) at low pH completely disrupts this

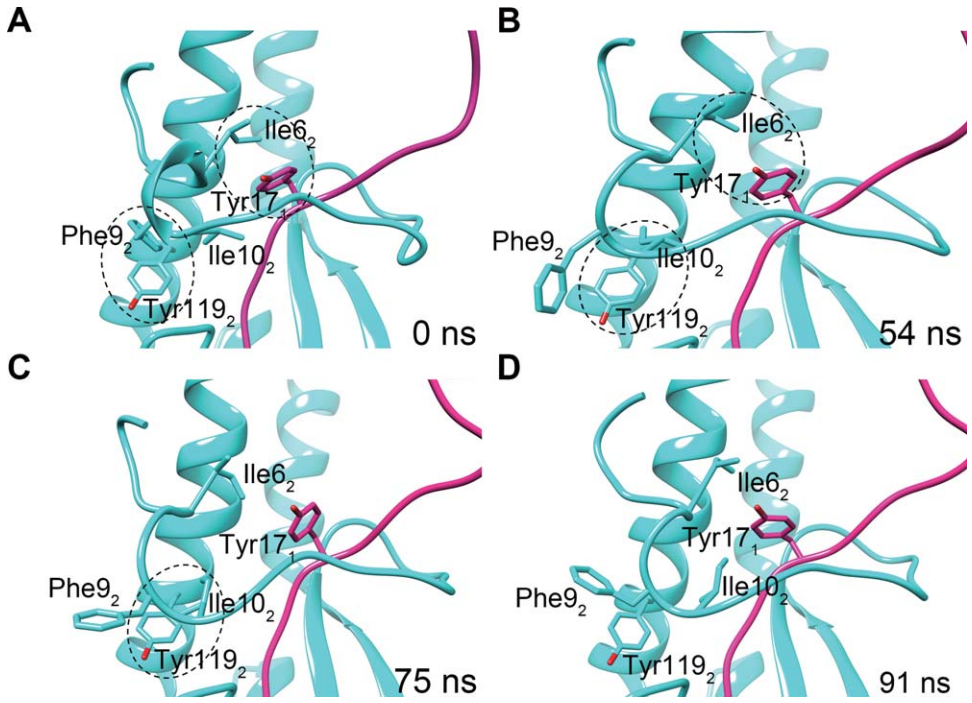

Figure 7

Hydrophobic barriers along the fusion peptide release pathway in H2 HA simulation at pH 4.5. Dashed circles indicate the hydrophobic interactions between fusion peptide and nearby residues. [Color figure can be viewed in the online issue, which is available at wileyonlinelibrary.com.]

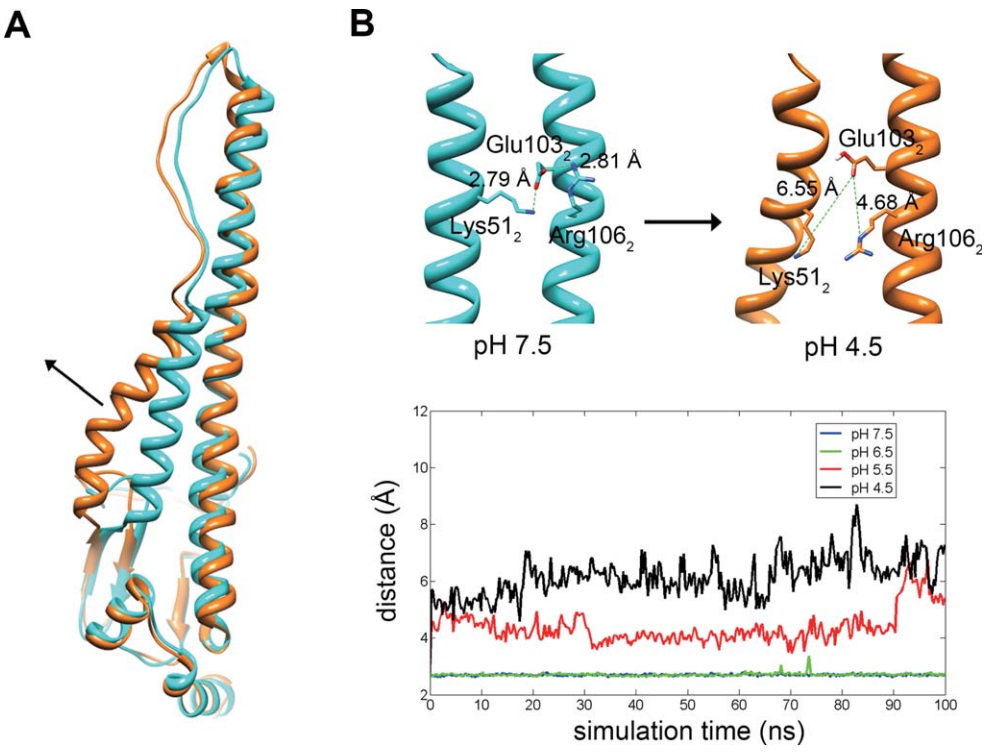

Figure 8

(**A**) Separation of short and long α-helices of H2 HA in low pH simulations. Simulation at pH 7.5 is shown in cyan and that at pH 4.5 is shown in orange. (**B**) Analysis of the salt-bridge distance between Glu103$_2$ and Lys51$_2$ at different pH conditions. [Color figure can be viewed in the online issue, which is available at wileyonlinelibrary.com.]

Table II
Calculated pK_a Values for H2 HA Titratable Residues at Different Stages[a]

Residues	First pKa prediction	Second pKa prediction	Third pKa prediction	Low pH intermediate
$His18_1$	4.7	7.8	7.3	6.0
$Glu89_1$	6.2	5.8	<4.5	5.6
$His184_1$	<4.5	5.7	6.7	<4.5
$His26_2$	5.6	7.3	6.8	5.5
$Glu74_2$	<4.5	4.5	4.7	4.8
$Asp109_2$	4.5	4.8	4.6	5.1
$His111_2$	4.5	6.5	5.3	5.2
$Asp112_2$	<4.5	<4.5	<4.5	<4.5

[a]First pK_a prediction is calculated based on neutral crystal structure; second pK_a prediction is calculated based on the last snapshot of 100 ns simulation at pH 4.5 with protonation state assigned according to first prediction results; third pK_a prediction is calculated based on the last snapshot of 100 ns simulation at pH 4.5 with protonation state assigned according to second prediction results.

favorable interaction, resulting a distance of 6.55 Å, thus assisting the separation of the short and long α-helices [Fig. 8(B)]. This is the prerequisite for the loop-to-helix transition of the interhelical loop and the relocation of short α-helix onto the long helix. Besides, the separation of the two helices further exposes the deeply buried fusion peptide and several late stage pH sensors, which are originally buried and silenced in the neutral pH structure (e.g., $His111_2$ and $Asp112_2$ as aforementioned).

There was only small conformational change in the B loop region over 100 ns simulations. However, disruption of the tetrad salt bridge network was observed. The protonation of $Glu89_1$ not only disrupt its own interaction with $Lys109_1$ and $Lys269_1$, but also perturb the whole tetrad network, releasing the $Glu69_2$ in the B loop (see the Supporting Information, Fig. S4).

Coupling between conformational change and protonation state

As noted previously, the lack of consideration for the coupling between the ionization equilibrium and the conformational dynamics limits us to the early stages of the structural reorganization. Here, we tried to improve our calculations by iteratively combining conventional MD simulation with pK_a predictions. Based on low pH simulation trajectories, we recalculated the pK_a values for each titratable residue and then carried out another 100 ns MD simulation with reassigned protonation states. We took three rounds of such iterations at pH 4.5 for H2 HA and obtained 300 ns simulation in total.

Indeed, we identified several extra protonated residues during our iterative simulation process which introduce more extensive structural reorganizations. Table II lists the calculated pK_a values of representative residues in H2 at different stages in comparison to the low-pH intermediate structure of the H2_HA2R106H mutant (results for all the residues are provided in Supporting Information, Table SIV and SV). Calculated pK_a shifts of these residues are consistent between the simulation snapshots and the crystal structure at intermediate state, which strongly supports our calculation results. $His18_1$ and $His26_2$ are identified as potential pH sensors in the initial fusion process and maintain their protonated states in the late stage. However, the initially deep buried residues $His184_1$, $Glu74_2$, $Asp109_2$, and $His111_2$ are gradually exposed along the iterative simulation process, and their calculated pK_a values are consistently up-shifted, which indicates that they might act as late stage pH sensors.

$Asp112_2$ was originally speculated to be protonated to destabilize its interactions with fusion peptide. However, the calculated pK_a values of $Asp112_2$ are all below 4.5 in our iterative pK_a calculations, which suggests that more extensive sampling might be required or transient protonation (calculated protonation probability of 0.12 at pH 4.5) might be adequate to disrupt the interactions. Thus, we manually protonated $Asp112_2$ and run 100 ns simulation. All the four hydrogen bonds are destroyed and the interaction with $Tyr14_2$ is also perturbed, resulting in the further release of the fusion peptide (see Supporting Information, Fig. S5). This is consistent with the experimental observation that mutation on $Asp112_2$ leads to a significantly elevated fusion pH.[18,23]

In the subsequent 200 ns simulation of H2 HA, we observed more extensive conformational change. The globular heads further dissociate from each other and completely detrimerize (see Supporting Information, movie S1). We also observed a significant conformational change of interhelical B loop (see Supporting Information, Fig. S6). Protonation of $Glu74_2$ and $Glu97_2$ disrupts the salt bridge locking interactions and loosen the clamped B loop. Rotation of the B loop exposes the originally well-packed $Phe63_2$, which agrees with the structural observation in the H2-HAR106H low-pH intermediate.[30] Beside, further exposure of $Phe70_2$, which has been previously proposed, was also captured. Relief of these structural restraints leads to the open conformation of B loop and this is prerequisite for the loop-to-helix transition. In our simulation, the released B loop has exhibited a propensity to form a helix structure. We run another long-time simulation (1 μs in total) of isolated B loop and found it spontaneously folded into a helix after 0.6 μs and remained stable throughout the simulation (see Supporting Information, movie S2). This further confirms the spring-loaded model and explains why no pH sensors have been identified on the B loop.

Comparison of different HA subtypes

There are now 18 known HA subtypes that can be divided into two phylogenetic groups (Supporting Information, Fig. S1). Sequence alignment shows that although the HA1 subunits vary greatly, the HA2 subunits are relatively conserved.[63] Besides H2 HA, we also

Table III
Comparison of Calculated pK_a Values for Potential pH Sensor Groups in Different HA Subtypes

		Glu1032 pH sensor groups				His181 pH sensor groups						
		$Glu103_2$	$Glu105_2$	$His106_2$	$Asp109_2$	$His18_1$	$His38_1$	$His111_2$	His262	Asp111	Glu891	Glu742
Group 1	H1	5.4	5.7	Arg	5.2	5.1	7.7	4.4	8.9	5.5	5.3	4.7
	H2	6.1	4.7	Arg	4.5	4.7	7.8	4.5	5.6	5.8	6.2	<4.5
	H5	6.1	5.0	Arg	4.5	6.3	7.5	4.7	7.7	5.7	4.8	5.0
	H9	5.7	Gln	Lys	<4.5	Gln	8.1	5.3	8.3	5.8	5.3	4.7
	H13	5.7	<4.5[a]	Lys	<4.5	Leu	Ser	5.7	8.2	5.0	5.5	4.6
Group 2	H3	6.3	Gln	5.7	<4.5	7.3	Asn	Thr	7.2	Ala	4.9	<4.5
	H7	6.5	Gln	5.0	<4.5	7.7	Asn	Ala	7.5	NA[b]	5.0	<4.5
	H14	5.7	Gln	6.4	<4.5	7.3	Ser	Thr	6.6	Phe	5.6	4.7

[a]In H13 HA, the residue at 105_2 position is Asp instead of Glu.
[b]In H7 HA, $Asp11_1$ has not been determined in selected crystal structure (1TI8).

carried out CPHMD for all the representative HA subtypes with available crystal structure (All pK_a calculation results are provided in Supporting Information, Table SVI–SXII). The overall change of charge distribution is similar in all HA subtypes. Although the titratable residues in globular head vary greatly in different HAs, all of them would be significantly positive charged at low pH in this region (see Supporting Information, Fig. S7), indicating that the overall effect of charge repulsion drives the globular head dissociation. The titratable residues in the stem region are more conserved. Many pH sensor groups identified in H2 HA are identical in all HA subtypes, while some are group-specific (see Table III and Supporting Information, Table SXIII).

$Glu103_2$ is identical in different HA subtypes and the calculated pK_a value of $Glu103_2$ has all been up-shifted. Thus, the protonation of $Glu103_2$ might be a common event to facilitate the separation of short and long α-helices in HA. However, adjacent residues at positions 105_2 and 106_2 display clade-specific amino acid combinations and distinct local conformations [Fig. 9(A)].[63] In most of group 1 HA subtypes, $Arg106_2$ points toward the threefold axis of the HA trimer, forming salt bridge interaction with $Glu103_2$. The crowding of the positive charges is alleviated by conserved acidic residues $Glu103_2$ and $Glu105_2$. According to our pK_a predictions, $Glu105_2$ is also protonated at low pH to further introduce charge repulsion to this region. In Group 2 HA subtypes, the residues at position 106_2 are histidines, and the imidazole rings rotate away from the central axis to form hydrogen bonds with $Lys51_2$ [Fig. 9(B)]. Such an orientation is more stable at fusion pH.[30] A neutral residue $Gln105_2$ replaces $Glu105_2$ in group 2 HA subtypes, and also in several group 1 HA subtypes.

$His18_1$ pH sensor group (including $His18_1$, $His38_1$, and $His111_2$) is only conserved in H1 clade HAs in group 1 (including H1, H2, H5, and H6). Mutation of $His18_1$ by Gln in H5 HA maintains the hydrogen bond with fusion peptide at low pH, and leads to a decreased fusion pH by 0.4 units.[28] For group two HAs, in the absence of $His38_1$, $His18_1$ flips up and loses the hydrogen bonds with $Met17_2$ of the fusion peptide [Fig. 9(C)]. Besides, we identified another potential pH sensor in group 2 HAs—$His17_1$. In neutral pH crystal structure, $His17_1$ forms water-bridged hydrogen bonds with the carbonyl oxygen of $Ala7_2$ and $Ile10_2$. While in group 1 HAs, residue at position 17_1 is tyrosine, which directly interacts with $Ala7_2$ and $Ile10_2$ [Fig. 9(C)]. Previous studies of H3 HA have shown that substitutions of $His17_1$ with Ala, Arg, or Glu, destroying the hydrogen bonding, resulting to an increased fusion pH ($\Delta pH = 0.4$, 0.7, and 0.9 respectively).[16,19,27] On contrast, substitution of $His17_1$ with Tyr would stabilize the H3 and led to a reduced fusion pH by 0.3 pH unit.[27] Thus, the water-mediated hydrogen bond network in group 2 HAs is likely to be disrupted by the protonation of $His17_1$ at low pH to facilitate the fusion peptide release, while tyrosine substitution at this position in group 1 HAs does not preserve this pH sensing function.

For other pH sensors, $His26_2$ and $Glu89_1$ are identical in all HA subtypes while $Asp11_1$ is only conserved in Group 1 HAs. The calculated pK_a values of these residues are similar in different subtypes. $Glu74_2$ is also identical in all HA subtypes. In H2 HA, our calculations have suggested that its pK_a will be up-shifted after the initial conformational change and act as a late-stage pH sensor. This is further confirmed in other HA subtypes. Several HA subtypes initially have up-shifted pK_a values for $Glu74_2$ (Table III).

We also carried out MD simulations for the H3 and H5 HAs. H5 is the closest clade member to H2 in phylogenetic and the dynamic behaviors are quite similar in our simulations (data not shown). However, H3 is in the other HA group and exhibits a different response to low pH environments in simulation. The globular head domains in H3 do not significantly dissociate and still pack against the HA2 subunit within the simulation time scale [Fig. 10(A)]. We cannot rule out the possibility that the dissociation will happen at a longer time scale, but the net charge calculation suggests that globular domains in H3 are more difficult to detrimerize. The change of net charge is more obvious in H2 [with net charge from

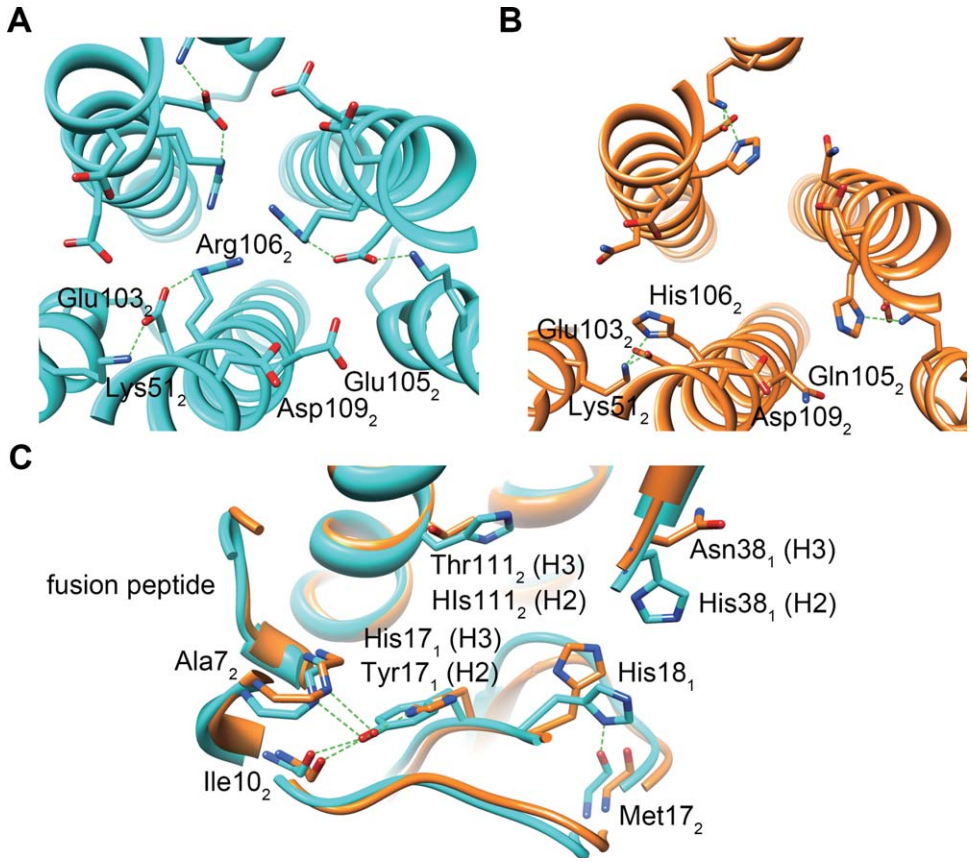

Figure 9

Comparison of pH sensor groups in group 1 (H2) and group 2 (H3) HA. H2 HA is color in cyan and H3 HA is color in orange. (**A** and **B**) Glu103$_2$ pH sensor group. (**C**) His18$_1$ pH sensor group. [Color figure can be viewed in the online issue, which is available at wileyonlinelibrary.com.]

0e to +14e, Fig. 2(B)] than that in H3 [with net charge from +7e to +16e, Fig. 10(C)]. Interestingly, the solvent exposure of the fusion peptides of H3 HA is more significant comparing with H2 HA [Fig. 10(B)]. As noted above, the absence of His18$_1$ hydrogen bonding, the additional pH sensor - His17$_1$, the reduced hydrophobic barrier by Y17$_1$H substitution, and the up-shifted pK$_a$ value of Asp112$_2$ may cooperatively contribute to the release of the fusion peptide in H3. This is also consistent with the experimental observation that the fusion peptide release may precede the detrimerization of the globular head domains in H3.[31,32,64] While the detrimerization process may occur before the release of fusion peptide in groups 1 HAs, such as H2 and H5, the structural transition triggered by low pH might take distinct routes in other HA subtypes.

Implication for the design of HA inhibitors

Influenza has presented a serious public health challenge, and new therapies are urgently needed to combat viruses which are resistant to current medicines or escape neutralization by the immune system. HA is an attractive candidate target for drug development as its essential roles during the virus infection. Recently, there has been particular interest in developing novel antibodies and small molecules targeting the stem region of HA, which is conserved in all HA subtypes and constitutes the core fusion machinery, to provide potent and broad fusion inhibition against various influenza viruses.[65–72] Identification of pH sensor groups and fusion pathways, especially in the early stages, holds the promise to rationally design HA inhibitors which could block the pH sensors and inhibit the conformational change induced by low pH. Here, we used representative antibody CR6261 and small molecule inhibitor TBHQ as examples to explore such inhibition mechanism and also proposed a novel pocket for the design of group specific HA inhibitors.

Antibody CR6261 was reported to recognize a highly conserved helical region and exhibit broad neutralization against group 1 HA influenza virus. It is well-positioned blow the hinge region to act as a molecular buttress to oppose the dissociation of the HA1 globular heads and inhibit membrane fusion.[65] We examined the structure

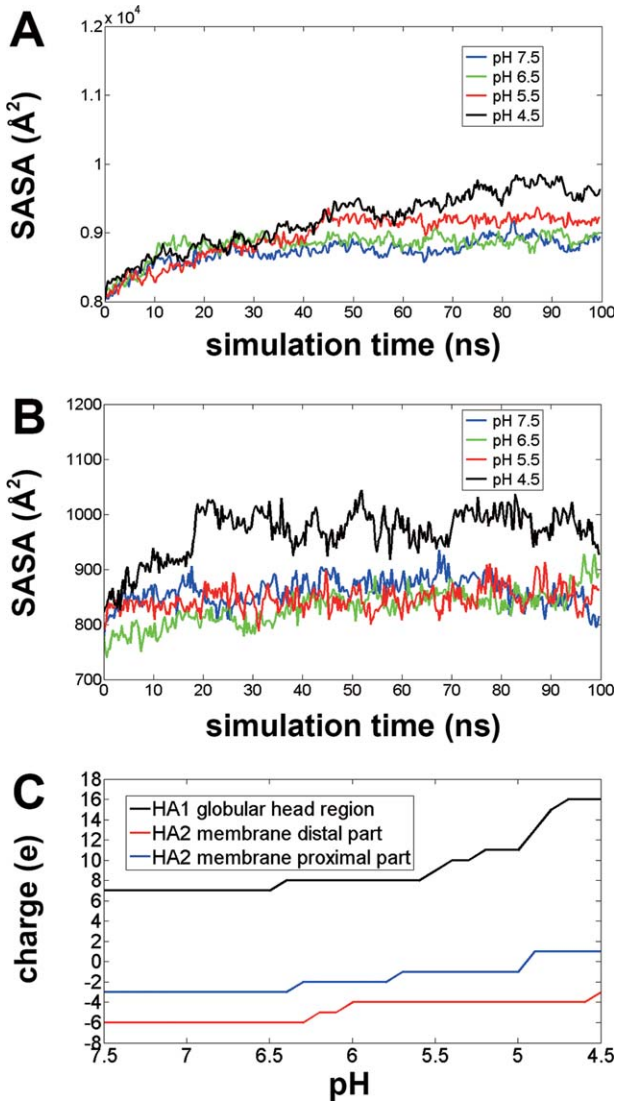

Figure 10

MD simulation of H3 HA. (**A**) Solvent accessible surface area (SASA) of globular head region during 100 ns simulations at different pH conditions. (**B**) SASA of fusion peptide (residues 1_2-20_2) during 100 ns simulations at different pH conditions. (**C**) Net charge of three specific regions in H3 HA as a function of pH. The color and residue selection are the same with those in H2 HA in Figure 1B. [Color figure can be viewed in the online issue, which is available at wileyonlinelibrary.com.]

and found it also binds adjacently to an important pH sensor group, the $His18_1$ group [as shown in Fig. 11(A)]. Binding of the antibody CR6261 completely buries this residue and would prevent its protonation in low pH. To confirm this speculation, we carried out CPHMD simulation on H5-CR6261 complex and found that the calculated pK_a value of $His18_1$ is down-shifted from 6.3 to 5.3, less feasible to be protonated. We believe the silence of this pH sensor group would contribute to the neutralization of CR6261. Similar silence mechanism has also been identified in broadly neutralizing antibodies F10 and CR8020 (see Supporting Information, Fig. S8).

TBHQ is a small molecule shown to stabilize several group 2 HAs and inhibit the low-pH-induced conformational change. It binds at the interface between the long and short α helices from neighboring monomers.[72] At the bottom of the TBHQ binding site, there is also a potential pH sensor, the $Glu103_2$ group [Fig. 11(B)]. We speculated that $Glu103_2$ becomes inaccessible to the solvent on TBHQ binding, and its protonation at low pH is inhibited. And this is consistent with the calculated pK_a value of $Glu103_2$, down-shifted from 6.3 to 5.8 in complex with TBHQ. It suggests that the fusion inhibition of TBHQ may be achieved not only by the favorable interactions with the neutral pH conformation of HA but also by blocking a critical pH sensor group which facilitates fusion pathway.

TBHQ binding site is only accessible in Group 2 HAs but blocked in Group 1 HAs due to an extra turn at the C terminus of the short a-helix (residues 56_2–68_2).[72] This additional turn of helix results from the formation of an intermonomer salt bridge between $Lys58_2$ and $Glu97_2$. However, searching for the structural differences between different HA groups, we have identified a novel pocket only exist in several Group 1 HAs (H2 and H5, see Supporting Information, Fig. S9). It is located between the interhelical loop and the loop from the HA1 globular domain. We carefully examined this novel pocket and found it resembling the TBHQ site in many ways. First, both sites locate at the interface of the neutral pH structure which should be disrupted for the structural reorganization. Therefore, small molecules binding at this region could potentially stabilize the neutral-pH structure. Second, a subtype-specific residue $His302_1$ locates at the bottom of this site, which is a potential pH sensor similar to the residue $Glu103_2$ in TBHQ site. Small molecules binding at this site could completely bury the pH sensor. In addition, this novel pocket is hydrophobic and rich in hydrogen bonding donor and acceptor groups. We expect that small molecules occupying at this novel pocket would attenuate the low-pH-induced conformational change by gluing the neutral pH structure.

CONCLUSIONS

We combined the CPHMD simulation with conventional MD simulation to study the pH-induced conformational change of HA. Our results describe a general mechanism for the structural reorganization pathway. Decreasing pH in the endosome alters the protonation states of many HA titratable residues, especially in the globular head regions. Increased positive charges (e.g., from 0e to +14e in H2 subtype) cause an enhancement of the electrostatic repulsive force and drive the

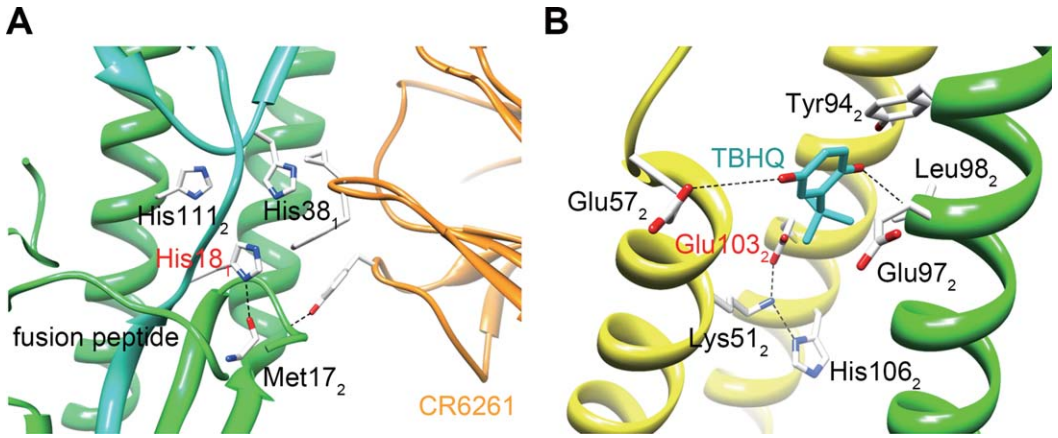

Figure 11

Silence mechanism of CR6261 and TBHQ. (**A**) Complex structure of H5 HA with antibody CR6261 (PDB ID: 3GBM). Binding of CR6261 blocks the potential pH sensor residue His18$_1$ and shift-down its pK_a value from 6.3 to 5.3. (**B**) Complex structure of H3 HA with small molecule inhibitor TBHQ (PDB ID: 3EYM). Binding of TBHQ buries the potential pH sensor residue Glu103$_2$ and shift-down its pK_a value from 6.3 to 5.8. [Color figure can be viewed in the online issue, which is available at wileyonlinelibrary.com.]

dissociation of HA1 globular head domains. Besides, several critical pH sensors are identified in HA2 stem region. Protonation of Glu103$_2$ and His18$_1$ facilitates the fusion peptide release, and protonation of Glu89$_1$ assists the interhelical B loop transition. The opening of globular head domains and separation of the short and long α-helices further expose the originally buried areas, where late-stage pH sensor groups are further protonated to accelerate this refolding process. Once the fusion peptide moves out of the cavity and the clamped B loop is released, the conformational change of loop-to-helix transition would happen spontaneously, which is known as spring-loaded model. Sequential activation of pH sensors leads to a cooperative and stepwise process of the pH-regulated HA conformational change.

Our calculations provided a better understanding of the experimental observations at atomistic details. Most identified pH sensor groups are consistent with the reported mutagenesis studies. Mutation of Asp109$_2$ disrupts the original hydrogen bond interactions with fusion peptide, thus elevates the fusion pH; while mutation of His18$_1$ by Gln maintains the hydrogen bond with fusion peptide at low pH, leads to a decreased fusion pH. We also predicted mutations of several potential pH sensors (such as Glu89$_1$ and Glu103$_2$) would alter the fusion pH, and experimental validations are desirable. Comparisons in different HA subtypes have identified subtype-specific pH sensor groups and distinct conformational change pathways, consistent with experimental observations that H2 and H3 subtypes exhibit different conformational states after exposure at low pH.[34] Our results would also shed light on developing novel therapeutic agents by targeting the key elements involving the pH-regulated conformational change. Blockage of critical pH sensor would contribute to the inhibition of the early stages of conformational change, as illustrated by antibody CR6261 and small molecule inhibitor TBHQ. A promising novel pocket has been identified in H2 and H5 HAs and would be particularly useful for developing fusion inhibitor against the deadly H5N1 influenza virus.

ACKNOWLEDGEMENTS

Computational support was provided by the Supercomputing Center of Chinese Academy of Sciences (SCCAS). We also thank Drs. Wenhui Li and Guocai Zhong at NIBS for their insightful suggestions in this study.

REFERENCES

1. Imai M, Watanabe T, Hatta M, Das SC, Ozawa M, Shinya K, Zhong G, Hanson A, Katsura H, Watanabe S, Li C, Kawakami E, Yamada S, Kiso M, Suzuki Y, Maher EA, Neumann G, Kawaoka Y. Experimental adaptation of an influenza H5 HA confers respiratory droplet transmission to a reassortant H5 HA/H1N1 virus in ferrets. Nature 2012;486(7403):420–428.
2. Xiong X, Coombs PJ, Martin SR, Liu J, Xiao H, McCauley JW, Locher K, Walker PA, Collins PJ, Kawaoka Y, Skehel JJ, Gamblin SJ. Receptor binding by a ferret-transmissible H5 avian influenza virus. Nature 2013;497(7449):392–396.
3. Zhang W, Shi Y, Lu X, Shu Y, Qi J, Gao GF. An airborne transmissible avian influenza H5 hemagglutinin seen at the atomic level. Science 2013;340(6139):1463–1467.
4. Herfst S, Schrauwen EJ, Linster M, Chutinimitkul S, de Wit E, Munster VJ, Sorrell EM, Bestebroer TM, Burke DF, Smith DJ, Rimmelzwaan GF, Osterhaus AD, Fouchier RA. Airborne transmission of influenza A/H5N1 virus between ferrets. Science 2012; 336(6088):1534–1541.
5. Fouchier RA, Schneeberger PM, Rozendaal FW, Broekman JM, Kemink SA, Munster V, Kuiken T, Rimmelzwaan GF, Schutten M, Van Doornum GJ, Koch G, Bosman A, Koopmans M, Osterhaus

AD. Avian influenza A virus (H7N7) associated with human conjunctivitis and a fatal case of acute respiratory distress syndrome. Proc Natl Acad Sci USA 2004;101(5):1356–1361.
6. Koopmans M, Wilbrink B, Conyn M, Natrop G, van der Nat H, Vennema H, Meijer A, van Steenbergen J, Fouchier R, Osterhaus A, Bosman A. Transmission of H7N7 avian influenza A virus to human beings during a large outbreak in commercial poultry farms in the Netherlands. Lancet 2004;363(9409):587–593.
7. Horby P. H7N9 is a virus worth worrying about. Nature 2013; 496(7446):399.
8. Richard M, Schrauwen EJ, de Graaf M, Bestebroer TM, Spronken MI, van Boheemen S, de Meulder D, Lexmond P, Linster M, Herfst S, Smith DJ, van den Brand JM, Burke DF, Kuiken T, Rimmelzwaan GF, Osterhaus AD, Fouchier RA. Limited airborne transmission of H7N9 influenza A virus between ferrets. Nature 2013;501(7468): 560–563.
9. Skehel JJ, Wiley DC. Receptor binding and membrane fusion in virus entry: the influenza hemagglutinin. Annu Rev Biochem 2000; 69:531–569.
10. Wilson IA, Skehel JJ, Wiley DC. Structure of the haemagglutinin membrane glycoprotein of influenza virus at 3 A resolution. Nature 1981;289(5796):366–373.
11. Bullough PA, Hughson FM, Skehel JJ, Wiley DC. Structure of influenza haemagglutinin at the pH of membrane fusion. Nature 1994; 371(6492):37–43.
12. Carr CM, Kim PS. A spring-loaded mechanism for the conformational change of influenza hemagglutinin. Cell 1993;73(4):823–832.
13. Carr CM, Chaudhry C, Kim PS. Influenza hemagglutinin is spring-loaded by a metastable native conformation. Proc Natl Acad Sci USA 1997;94(26):14306–14313.
14. Huang Q, Opitz R, Knapp EW, Herrmann A. Protonation and stability of the globular domain of influenza virus hemagglutinin. Biophys J 2002;82(2):1050–1058.
15. Choi HS, Huh J, Jo WH. Electrostatic energy calculation on the pH-induced conformational change of influenza virus hemagglutinin. Biophys J 2006;91(1):55–60.
16. Daniels RS, Downie JC, Hay AJ, Knossow M, Skehel JJ, Wang ML, Wiley DC. Fusion mutants of the influenza virus hemagglutinin glycoprotein. Cell 1985;40(2):431–439.
17. Doms RW, Gething MJ, Henneberry J, White J, Helenius A. Variant influenza virus hemagglutinin that induces fusion at elevated pH. J Virol 1986;57(2):603–613.
18. Gething MJ, Doms RW, York D, White J. Studies on the mechanism of membrane fusion: site-specific mutagenesis of the hemagglutinin of influenza virus. J Cell Biol 1986;102(1):11–23.
19. Wharton SA, Skehel JJ, Wiley DC. Studies of influenza haemagglutinin-mediated membrane fusion. Virology 1986;149(1): 27–35.
20. Steinhauer DA, Wharton SA, Skehel JJ, Wiley DC, Hay AJ. Amantadine selection of a mutant influenza virus containing an acid-stable hemagglutinin glycoprotein: evidence for virus-specific regulation of the pH of glycoprotein transport vesicles. Proc Natl Acad Sci USA 1991;88(24):11525–11529.
21. Steinhauer DA, Wharton SA, Skehel JJ, Wiley DC. Studies of the membrane fusion activities of fusion peptide mutants of influenza virus hemagglutinin. J Virol 1995;69(11):6643–6651.
22. Lin YP, Wharton SA, Martin J, Skehel JJ, Wiley DC, Steinhauer DA. Adaptation of egg-grown and transfectant influenza viruses for growth in mammalian cells: selection of hemagglutinin mutants with elevated pH of membrane fusion. Virology 1997;233(2):402–410.
23. Cross KJ, Wharton SA, Skehel JJ, Wiley DC, Steinhauer DA. Studies on influenza haemagglutinin fusion peptide mutants generated by reverse genetics. EMBO J 2001;20(16):4432–4442.
24. Ilyushina NA, Govorkova EA, Russell CJ, Hoffmann E, Webster RG. Contribution of H7 haemagglutinin to amantadine resistance and infectivity of influenza virus. J Gen Virol 2007;88(Pt 4):1266–1274.
25. Rachakonda PS, Veit M, Korte T, Ludwig K, Bottcher C, Huang Q, Schmidt MF, Herrmann A. The relevance of salt bridges for the stability of the influenza virus hemagglutinin. FASEB J 2007;21(4):995–1002.
26. Casali M, Banta S, Zambonelli C, Megeed Z, Yarmush ML. Site-directed mutagenesis of the hinge peptide from the hemagglutinin protein: enhancement of the pH-responsive conformational change. Protein Eng Des Sel 2008;21(6):395–404.
27. Thoennes S, Li ZN, Lee BJ, Langley WA, Skehel JJ, Russell RJ, Steinhauer DA. Analysis of residues near the fusion peptide in the influenza hemagglutinin structure for roles in triggering membrane fusion. Virology 2008;370(2):403–414.
28. Reed ML, Yen HL, DuBois RM, Bridges OA, Salomon R, Webster RG, Russell CJ. Amino acid residues in the fusion peptide pocket regulate the pH of activation of the H5N1 influenza virus hemagglutinin protein. J Virol 2009;83(8):3568–3580.
29. Reed ML, Bridges OA, Seiler P, Kim JK, Yen HL, Salomon R, Govorkova EA, Webster RG, Russell CJ. The pH of activation of the hemagglutinin protein regulates H5N1 influenza virus pathogenicity and transmissibility in ducks. J Virol 2010;84(3):1527–1535.
30. Xu R, Wilson IA. Structural characterization of an early fusion intermediate of influenza virus hemagglutinin. J Virol 2011;85(10): 5172–5182.
31. White JM, Wilson IA. Anti-peptide antibodies detect steps in a protein conformational change: low-pH activation of the influenza virus hemagglutinin. J Cell Biol 1987;105(6 Pt 2):2887–2896.
32. Steinhauer DA, Martin J, Lin YP, Wharton SA, Oldstone MB, Skehel JJ, Wiley DC. Studies using double mutants of the conformational transitions in influenza hemagglutinin required for its membrane fusion activity. Proc Natl Acad Sci USA 1996;93(23):12873–12878.
33. Bottcher C, Ludwig K, Herrmann A, van Heel M, Stark H. Structure of influenza haemagglutinin at neutral and at fusogenic pH by electron cryo-microscopy. FEBS Lett 1999;463(3):255–259.
34. Puri A, Booy FP, Doms RW, White JM, Blumenthal R. Conformational changes and fusion activity of influenza virus hemagglutinin of the H2 and H3 subtypes: effects of acid pretreatment. J Virol 1990;64(8):3824–3832.
35. Lee MS, Salsbury FR, Jr., Brooks CL, III. Constant-pH molecular dynamics using continuous titration coordinates. Proteins 2004; 56(4):738–752.
36. Khandogin J, Brooks CL, III. Constant pH molecular dynamics with proton tautomerism. Biophys J 2005;89(1):141–157.
37. Khandogin J, Brooks CL, III. Toward the accurate first-principles prediction of ionization equilibria in proteins. Biochemistry 2006; 45(31):9363–9373.
38. Tong S, Li Y, Rivailler P, Conrardy C, Castillo DA, Chen LM, Recuenco S, Ellison JA, Davis CT, York IA, Turmelle AS, Moran D, Rogers S, Shi M, Tao Y, Weil MR, Tang K, Rowe LA, Sammons S, Xu X, Frace M, Lindblade KA, Cox NJ, Anderson LJ, Rupprecht CE, Donis RO. A distinct lineage of influenza A virus from bats. Proc Natl Acad Sci USA 2012;109(11):4269–4274.
39. Tong S, Zhu X, Li Y, Shi M, Zhang J, Bourgeois M, Yang H, Chen X, Recuenco S, Gomez J, Chen LM, Johnson A, Tao Y, Dreyfus C, Yu W, McBride R, Carney PJ, Gilbert AT, Chang J, Guo Z, Davis CT, Paulson JC, Stevens J, Rupprecht CE, Holmes EC, Wilson IA, Donis RO. New world bats harbor diverse influenza a viruses. PLoS Pathog 2013;9(10):e1003657.
40. Berman HM, Westbrook J, Feng Z, Gilliland G, Bhat TN, Weissig H, Shindyalov IN, Bourne PE. The protein data bank. Nucleic Acids Res 2000;28(1):235–242.
41. Lu X, Shi Y, Gao F, Xiao H, Wang M, Qi J, Gao GF. Insights into avian influenza virus pathogenicity: the hemagglutinin precursor HA0 of subtype H16 has an alpha-helix structure in its cleavage site with inefficient HA1/HA2 cleavage. J Virol 2012;86(23):12861–12870.
42. Sun X, Shi Y, Lu X, He J, Gao F, Yan J, Qi J, Gao GF. Bat-derived influenza hemagglutinin H17 does not bind canonical avian or

human receptors and most likely uses a unique entry mechanism. Cell Rep 2013;3(3):769–778.
43. Zhu X, Yu W, McBride R, Li Y, Chen LM, Donis RO, Tong S, Paulson JC, Wilson IA. Hemagglutinin homologue from H17N10 bat influenza virus exhibits divergent receptor-binding and pH-dependent fusion activities. Proc Natl Acad Sci USA 2013;110(4): 1458–1463.
44. Nicholls H. Pandemic influenza: the inside story. PLoS Biol 2006; 4(2):e50.
45. Zhang W, Shi Y, Lu X, Shu Y, Qi J, Gao GF. An airborne transmissible avian influenza h5 hemagglutinin seen at the atomic level. Science 2013;340(6139):1463–1467.
46. Brooks BR, Bruccoleri RE, Olafson BD, States DJ, Swaminathan S, Karplus M. CHARMM: A program for macromolecular energy, minimization, and dynamics calculations. J Comput Chem 1983;4(2):187–217.
47. Feig M, Karanicolas J, Brooks CL, III. MMTSB Tool Set: enhanced sampling and multiscale modeling methods for applications in structural biology. J Mol Graph Model 2004;22(5):377–395.
48. Mackerell AD, Bashford JD, M. Karplus. All-atom empirical potential for molecular modeling and dynamics studies of proteins. J Phys Chem 1998;102(18):3586–3616.
49. Feig M, Mackerell AD, Brooks CL. Force field influence on the observation of π-helical protein structures in molecular dynamics simulations. J Phys Chem B 2003;107(12):2831–2836.
50. Chen J, Im W, Brooks CL, III. Balancing solvation and intramolecular interactions: toward a consistent generalized Born force field. J Am Chem Soc 2006;128(11):3728–3736.
51. Andersen HC. A "velocity" version of the shake algorithm for molecular dynamics calculations. J Comput Phys 1983;52(1):24–34.
52. Vanommeslaeghe K, MacKerell AD, Jr. Automation of the CHARMM General Force Field (CGenFF) I: bond perception and atom typing. J Chem Inf Model 2012;52(12):3144–3154.
53. Vanommeslaeghe K, Raman EP, MacKerell AD, Jr. Automation of the CHARMM general force field (CGenFF) II: assignment of bonded parameters and partial atomic charges. J Chem Inf Model 2012;52(12):3155–3168.
54. Bowers KJ, Chow E, Shaw DE. Scalable algorithms for molecular dynamics simulations on commodity clusters. In: Proceedings of the ACM/IEEE Conference on Supercomputing (SC06). Florida.
55. Berendsen HJC, Postma JPM, Gunsteren WFv, DiNola A, JR Haak. Molecular dynamics with coupling to an external bath. J Chem Phys 1984;81(8):3684–3690.
56. Darden T, York D, Pedersen L. Particle mesh Ewald: An Nlog(N) method for Ewald sums in large systems. J Chem Phys 1993;98(12): 10089–10092.
57. Pettersen EF, Goddard TD, Huang CC, Couch GS, Greenblatt DM, Meng EC, Ferrin TE. UCSF Chimera: a visualization system for exploratory research and analysis. J Comput Chem 2004;25(13):1605–1612.
58. Humphrey W, Dalke A, Schulten K. VMD: visual molecular dynamics. J Mol Graph 1996;14(1):33–38, 27–38.
59. Kampmann T, Mueller DS, Mark AE, Young PR, Kobe B. The role of histidine residues in low-pH-mediated viral membrane fusion. Structure 2006;14(10):1481–1487.
60. Mueller DS, Kampmann T, Yennamalli R, Young PR, Kobe B, Mark AE. Histidine protonation and the activation of viral fusion proteins. Biochem Soc Trans 2008;36(Pt 1):43–45.
61. Baker NA, Sept D, Joseph S, Holst MJ, McCammon JA. Electrostatics of nanosystems: application to microtubules and the ribosome. Proc Natl Acad Sci USA 2001;98(18):10037–10041.
62. Tamm LK. Hypothesis: spring-loaded boomerang mechanism of influenza hemagglutinin-mediated membrane fusion. Biochim Biophys Acta 2003;1614(1):14–23.
63. Russell RJ, Gamblin SJ, Haire LF, Stevens DJ, Xiao B, Ha Y, Skehel JJ. H1 and H7 influenza haemagglutinin structures extend a structural classification of haemagglutinin subtypes. Virology 2004; 325(2):287–296.
64. Leikina E, Ramos C, Markovic I, Zimmerberg J, Chernomordik LV. Reversible stages of the low-pH-triggered conformational change in influenza virus hemagglutinin. EMBO J 2002;21(21):5701–5710.
65. Ekiert DC, Bhabha G, Elsliger MA, Friesen RH, Jongeneelen M, Throsby M, Goudsmit J, Wilson IA. Antibody recognition of a highly conserved influenza virus epitope. Science 2009;324(5924): 246–251.
66. Fleishman SJ, Whitehead TA, Ekiert DC, Dreyfus C, Corn JE, Strauch EM, Wilson IA, Baker D. Computational design of proteins targeting the conserved stem region of influenza hemagglutinin. Science 2011;332(6031):816–821.
67. Ekiert DC, Friesen RH, Bhabha G, Kwaks T, Jongeneelen M, Yu W, Ophorst C, Cox F, Korse HJ, Brandenburg B, Vogels R, Brakenhoff JP, Kompier R, Koldijk MH, Cornelissen LA, Poon LL, Peiris M, Koudstaal W, Wilson IA, Goudsmit J. A highly conserved neutralizing epitope on group 2 influenza A viruses. Science 2011;333(6044): 843–850.
68. Dreyfus C, Laursen NS, Kwaks T, Zuijdgeest D, Khayat R, Ekiert DC, Lee JH, Metlagel Z, Bujny MV, Jongeneelen M, van der Vlugt R, Lamrani M, Korse HJ, Geelen E, Sahin O, Sieuwerts M, Brakenhoff JP, Vogels R, Li OT, Poon LL, Peiris M, Koudstaal W, Ward AB, Wilson IA, Goudsmit J, Friesen RH. Highly conserved protective epitopes on influenza B viruses. Science 2012;337(6100): 1343–1348.
69. Corti D, Voss J, Gamblin SJ, Codoni G, Macagno A, Jarrossay D, Vachieri SG, Pinna D, Minola A, Vanzetta F, Silacci C, Fernandez-Rodriguez BM, Agatic G, Bianchi S, Giacchetto-Sasselli I, Calder L, Sallusto F, Collins P, Haire LF, Temperton N, Langedijk JP, Skehel JJ, Lanzavecchia A. A neutralizing antibody selected from plasma cells that binds to group 1 and group 2 influenza A hemagglutinins. Science 2011;333(6044):850–856.
70. Whitehead TA, Chevalier A, Song Y, Dreyfus C, Fleishman SJ, De Mattos C, Myers CA, Kamisetty H, Blair P, Wilson IA, Baker D. Optimization of affinity, specificity and function of designed influenza inhibitors using deep sequencing. Nat Biotechnol 2012;30(6): 543–548.
71. Sui J, Hwang WC, Perez S, Wei G, Aird D, Chen LM, Santelli E, Stec B, Cadwell G, Ali M, Wan H, Murakami A, Yammanuru A, Han T, Cox NJ, Bankston LA, Donis RO, Liddington RC, Marasco WA. Structural and functional bases for broad-spectrum neutralization of avian and human influenza A viruses. Nat Struct Mol Biol 2009;16(3):265–273.
72. Russell RJ, Kerry PS, Stevens DJ, Steinhauer DA, Martin SR, Gamblin SJ, Skehel JJ. Structure of influenza hemagglutinin in complex with an inhibitor of membrane fusion. Proc Natl Acad Sci USA 2008;105(46):17736–17741.